Developing compact and innovative dual-band thermal imagers using multi-layer diffractive optical elements

Laborde, Victor ; Loicq, J.J.D.; Habraken, Serge

DOI
10.1117/12.2630169

Publication date
2022

Document Version
Final published version

Published in
Space Telescopes and Instrumentation 2022

PROCEEDINGS OF SPIE

SPIEDigitalLibrary.org/conference-proceedings-of-spie

Developing compact and innovative dual-band thermal imagers using multi-layer diffractive optical elements

Victor Laborde, Jérôme Loicq, Serge Habraken

Victor Laborde, Jérôme Loicq, Serge Habraken, "Developing compact and innovative dual-band thermal imagers using multi-layer diffractive optical elements," Proc. SPIE 12180, Space Telescopes and Instrumentation 2022: Optical, Infrared, and Millimeter Wave, 121805Q (27 August 2022); doi: 10.1117/12.2630169

SPIE.

Event: SPIE Astronomical Telescopes + Instrumentation, 2022, Montréal, Québec, Canada

Developing compact and innovative dual-band thermal imagers using multi-layer diffractive optical elements

Victor LABORDE[1], Jérôme LOICQ[1,2], and Serge HABRAKEN[1]

[1]Centre Spatial de Liege, Avenue du Pré-Aily, 4031 Angleur, Belgium
[2]Faculty of Aerospace Engineering, Delft University of Technology, Kluyverweg 1, 2629 HS Delft, Netherlands

ABSTRACT

Infrared (IR) remote sensing offers a huge range of applications, mostly addressing make-or-break issues of our century (wildfires, irrigation monitoring, etc.). Multispectral spaceborne instruments require bulky optical systems designed for a specific scientific goal and have very low revisit time. Thereby, constellations of small satellites embarking compact dual-band IR imagers are very promising solutions. We study a dual-band IR diffractive element called multilayer diffractive optical elements (MLDOE). It replaces classical diffractive lenses (DOEs) that cannot operate simultaneously in two distinct wavebands. An MLDOE design is studied using the rigorous finite difference time domain (FDTD) method. Its performance at the "best" focal plane is deduced using free-space Fourier optics wave propagation. The presented MLDOE design has over 80% Strehl ratio in both bands, outperforming classical DOEs. Its chromatic focal shift has a negative variation, in opposition to refractive lenses, allowing efficient and compact dual-band hybrid lenses.

Keywords: Dual-band infrared, Earth observation, Diffractive optics, FDTD, Fourier optics

1. INTRODUCTION

Multispectral spaceborne instruments are of great interest for Earth observation: they provide ground coverage and generate high-value scientific data. However, they require bulky optical systems designed for a specific scientific goal. For monitoring purposes in the thermal infrared (IR) domain, dual-band instruments are often sufficient,[1,2] provided that their revisit time is less than two days. This is achievable using constellations of small satellites, which sets the need for compact dual-band infrared imagers. We consider two infrared wavebands, defined by the atmospheric IR windows: the mid-wave infrared (MWIR) from 3 to 5 µm and the long-wave infrared (LWIR) from 8 to 12 µm. The MWIR band is often shortened (4.4–5 µm) to avoid solar albedo contributions.

Refractive systems are rendered more compact when combined with extremely thin diffractive lenses. In addition, these diffractive optical elements (DOEs) very well compensate for the chromatic and thermal defocuses of refractive lenses. However, conventional monolayer DOEs cannot be used for dual-band IR applications since they can only operate within a narrow spectral band. The promising solution studied in this paper consists of an extended dual-band DOE called multilayer diffractive optical element (MLDOE). This optical component has been intensively studied since 1997.[3] The extended scalar theory (EST), introduced by Swanson[4] and recently applied to MLDOEs[5] combines the grating equation and Snell's law to optimize the profile of a DOE (reducing the shadowing effect). Finally, FDTD and Fourier optics have been combined to accurately estimate MLDOE's optical performance at the focal plane.[6]

In this article, we explain how to retrieve an MLDOE performance and how to optimize its shape using the EST (Sec. 2). Since MLDOEs are complex diffractive elements, we describe a process to accurately retrieve the optical performance at the focal plane. This procedure combines an FDTD-based phase model (Section 3.1) with Fourier optics (Section 3.2). An MLDOE's optical performance is computed at its "best" focal plane and evaluated over the MWIR-LWIR wavebands using the Strehl ratio metric. As a result, an MLDOE with optimized profile design is tested in both bands and compared to a classical ZnS 4 DOE.

Further author information: (Send correspondence to Victor Laborde)
Victor Laborde: E-mail: victor.laborde@uliege.be
Loicq Jérôme: E-mail: J.J.D.Loicq@tudelft.nl

Space Telescopes and Instrumentation 2022: Optical, Infrared, and Millimeter Wave, edited by Laura E. Coyle, Shuji Matsuura, Marshall D. Perrin, Proc. of SPIE Vol. 12180, 121805Q · © 2022 SPIE · 0277-786X · doi: 10.1117/12.2630169

2. MLDOE EST DESIGN

An MLDOE is composed of two harmonic diffractive optical elements (HDOEs)[7,8] (Fig. 1), joined together by an optical material or separated by air. These HDOEs are made of different materials, and their groove heights are designed to provide constructive interference for two distinct wavelengths, called "design wavelengths" and denoted λ_1 and λ_2. Both layers are aligned and have the same groove periods (i.e., the same number of diffractive zones). As an example, a three-layer MLDOE made of IRG24-IRG27-AgCl is depicted in Fig. 1:

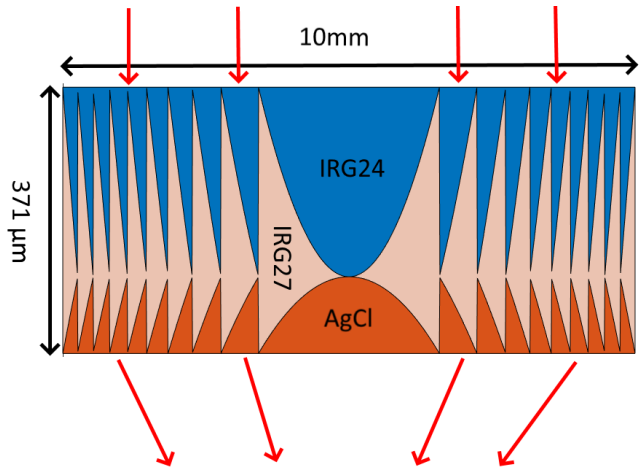

Figure 1: IRG24-IRG27-AgCl three-layer MLDOE layout. The incident light is displayed by red arrows.

This section describes the extended scalar theory (EST), introduced by Swanson,[4] and its application to MLDOEs.[5] By combining Snell's law of refraction and the grating equation, the EST method provides optimal thickness for each diffractive groove, which reduces the shadowing effect (unwanted shielding of light by the grooves).

Following this reasoning, alternative MLDOE layer thickness equations has been proposed.[5] They are based on the layout depicted in Fig. 2.

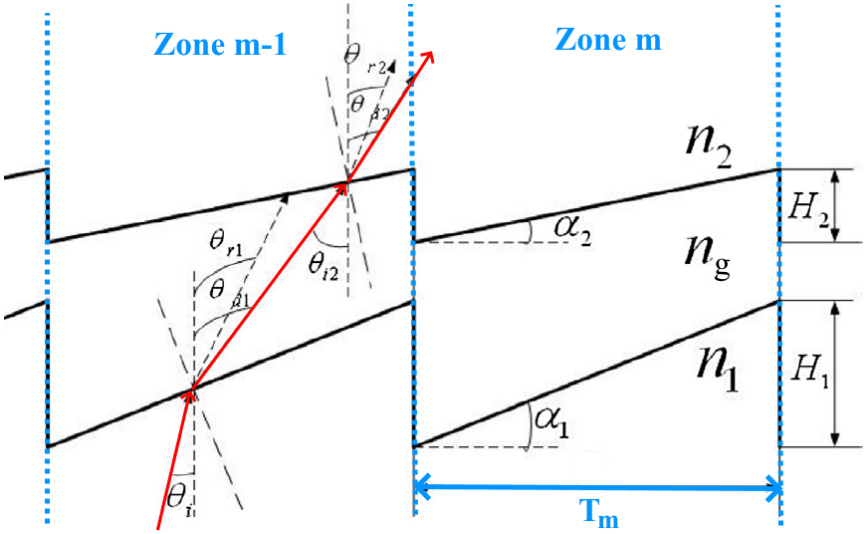

Figure 2: Extended scalar theory applied to an MLDOE (adapted from:[5]). The deviation angle θ_d is obtained using the local grating equation while θ_r results from Snell's law. Initially, the layer heights H_1 and H_2 are constant, given by the TEA. EST alternative profile heights are obtained when $\theta_d = \theta_r$ for both layers. T_m is the mth zone period. The light trajectory is displayed in red.

Following Fig. 2 layout, we define n_1, n_g and n_2 the refractive indices of layer 1, the gap and layer 2, respectively. The period size T_m varies for each zone m according to.[9] $\alpha_1 = H_1/T_m$ and $\alpha_2 = H_2/T_m$, with H_1 and H_2 the initial microstructure heights of layer 1 and 2. H_1 and H_2 are initially computed using the thin element approximation (TEA) as described in:[5,6]

$$\begin{cases} H_1 = \dfrac{\lambda_2 A(\lambda_1) - \lambda_1 A(\lambda_2)}{B(\lambda_1)A(\lambda_2) - B(\lambda_2)A(\lambda_1)} \\ H_2 = \dfrac{\lambda_1 B(\lambda_2) - \lambda_2 B(\lambda_1)}{B(\lambda_1)A(\lambda_2) - B(\lambda_2)A(\lambda_1)} \end{cases} \tag{1}$$

where $A(\lambda) = n_2(\lambda) - n_g(\lambda)$ and $B(\lambda) = n_1(\lambda) - n_g(\lambda)$. The wavelengths λ_1 and λ_2 are the MLDOE design wavelengths, defined in two distinct wavebands. The EST height calculation for the first layer is detailed in the following.

Snell's law of refraction is applied to the first layer:

$$n_1 \sin(\theta_i + \alpha_1) = n_g \sin(\theta_{r1} + \alpha_1) \tag{2}$$

θ_i and θ_{r1} are respectively the incident and refracted angles. The grating equation, applied to the first layer at local period T_m, wavelength λ and diffractive order p_1, gives:

$$n_g(\lambda)\sin\theta_{d1} - n_1(\lambda)\sin\theta_i = \frac{p_1\lambda}{T_m} \tag{3}$$

for a particular wavelength $\lambda = \lambda_{opt}$ and order p_1, we can equate the refractive and diffractive deviation angles ($\theta_{d1} = \theta_{r1}$) in Eq. 3. It results in a single layer height value, $H_1^{EST}(T_m)$, for each zone m of layer 1:

$$H_1^{EST}(T_m) = \frac{p_1\lambda_{opt}}{n_1\cos\theta_i - \sqrt{n_g^2 - \left(\dfrac{p_1\lambda_{opt}}{T_m} + n_1\sin\theta_i\right)^2}} \tag{4}$$

the MLDOE layer height depends on the chosen "optimization" wavelength λ_{opt} and the chosen operating order p_1. Refractive indices in Eq. 4 are defined at λ_{opt}. The second layer EST height $H_2^{EST}(T_m)$ follows a similar calculation, detailed in:[5]

$$H_2^{EST}(T_m) = \frac{p_2\lambda_{opt}}{\sqrt{n_2^2 - \left(\dfrac{(p_1+p_2)\lambda_{opt}}{T_m} + n_1\sin\theta_i\right)^2} - \sqrt{n_g^2 - \left(\dfrac{p_1\lambda_{opt}}{T_m} + n_1\sin\theta_i\right)^2}} \tag{5}$$

where p_2 corresponds to the operating diffractive order of layer 2. Since this paper focuses on the on-axis MLDOE design and performance, we assume $\theta_i = 0°$ in the following.

Each MLDOE diffractive zone m will have a unique thickness $H_{EST}(T_m)$. Eq. 5 supposes that $p_1 + p_2 = 1$, which is imposed in this whole paper to ensure that the studied MLDOE designs are converging (first order). The diffractive orders p_1 and p_2 are expressed in,[5] based on the harmonic diffractive optical elements (HDOEs) theory:[7,8]

$$\begin{cases} p_1 = \dfrac{H_1}{\lambda_{opt}}[n_1(\lambda_{opt}) - n_g(\lambda_{opt})] \\ p_2 = \dfrac{H_2}{\lambda_{opt}}[n_2(\lambda_{opt}) - n_g(\lambda_{opt})] \\ \Rightarrow p_1 + p_2 = 1 \end{cases} \tag{6}$$

the relation $p_1 + p_2 = 1$ is ensured using the TEA heights definition of Eq. 1.

3. MONOCHROMATIC STREHL RATIO SIMULATION

In this section, we detail a procedure to retrieve the Strehl ratio and the focal length of any MLDOE design. In the whole article, we use the Strehl ratio at the "best" focal plane as the main MLDOE optical performance metric. This simulation process has been introduced in[6] and is depicted in Fig. 3:

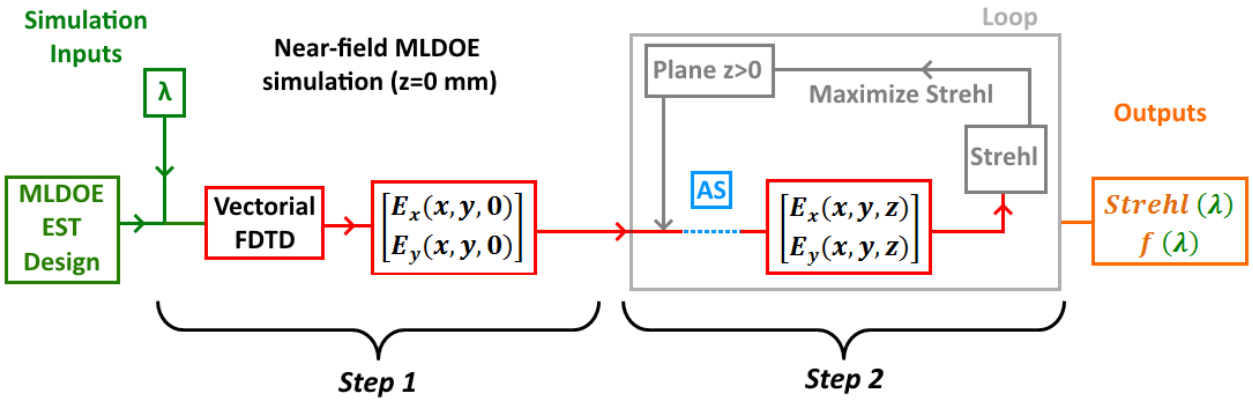

Figure 3: Diagram showing the hybrid procedure used in this paper to retrieve the Strehl ratio and the focal length of any MLDOE design. This procedure is divided into two steps: 1) modeling the MLDOE near-field using FDTD and 2) using Fourier optics (angular spectrum AS) in free-space to retrieve the two above-mentioned outputs.

The Strehl ratio retrieval procedure depicted in Fig. 3 combines near-field modeling (step 1) and free-space optical propagation (step 2). The former is detailed in Section 3.1 and involves a rigorous vectorial electromagnetic approach (FDTD). The optical propagation in free-space is described in Section 3.2 and revolves around Fourier optics, specifically the angular spectrum of plane waves. The procedure depicted in Fig. 3 takes an MLDOE design as input (i.e. the periods T_m and thicknesses $H_{T_m}^{EST}$ for any zone m) and is purely monochromatic. The loop, displayed in gray, allows to precisely determine the "best" focal plane $f(\lambda)$.

The focal plane of an MLDOE is theoretically given by the following law, whose expression is the same as for standard DOEs:[9]

$$f_j(\lambda) = D\frac{F/\sharp}{j\lambda} \tag{7}$$

where j is the diffractive order ($j = 1$ is considered in this paper).

However, since this law has been demonstrated using the TEA, it might be inaccurate for thick MLDOEs. Consequently, the "best" focal plane is considered unknown in this paper. Concentrating on the loop, displayed in gray in Fig. 3, each optical propagation to any plane $z > 0$ leads to a Strehl ratio. Therefore, the "best" focal plane $f(\lambda)$ is defined as the plane with the highest Strehl ratio output and is determined iteratively.

3.1 MLDOE near-field modeling with FDTD

FDTD wave simulation is performed using OptiFDTD software.[10] Starting from a plane wave, a complex electric field is propagated numerically through the MLDOE. Only the E_x and E_y components are considered, the E_z component being negligible, as it is along the propagation direction. The circular symmetry of the problem is used to reduce the sampling effort needed. The most adequate sampling is studied in the worst-case scenario: low F-number (F/10), high material index (Germanium) and low wavelength ($\lambda = 4.4$ µm). Fig. 4a) shows the sampling convergence curve, obtained by computing the Strehl ratio at the focal plane, based on the built-in FDTD far-field calculator, for each sampling trial.

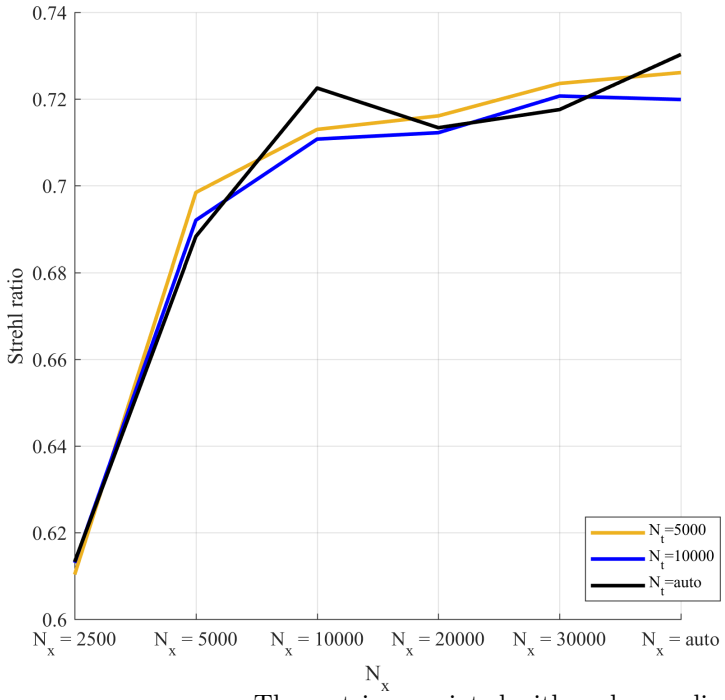

Figure 4: FDTD sampling convergence curve. The metric associated with each sampling trial is the Strehl ratio, computed at the "best" focal plane. The sampling along the optical axis (N_z, δ_z), as well as the radial and time sampling steps δ_x and δ_t are automatically computed by the OptiFDTD software ("auto setup"). N_x is the number of samples in the radial dimension (perpendicular to wave propagation direction z) and N_t is the number of time steps.

As a result of Fig. 4, we select the following sampling: $N_x = 20000$ and $N_t = 5000$, which is sufficient even in a worst-case scenario. All FDTD simulations performed in this article are therefore considered exact.

3.2 Angular spectrum free space propagation

This section details how Fourier optics propagation (Fig. 3 step 2: AS) is performed in this paper. Analysis using the Fourier transform formalism is a powerful optical modeling tool introduced and widely popularized by Goodman.[11] It provides a straightforward method for evaluating, in any point in space, the properties (phase and amplitude) of a monochromatic electromagnetic wave, propagating in a free-space medium (linear, homogeneous, non-magnetic, free of electric charge and current). More specifically, the accurate angular spectrum (AS) method is used in this paper for optical wave propagation. A complex field phasor $U(x, y; z)$ can be expressed at any propagation plane z along the optical axis, as long as the initial phasor $U(x, y; 0)$ is known:

$$\begin{cases} U(x,y;z) = \mathcal{F}^{-1}\{\mathcal{F}\{U(x,y;0)\}H_z(f_x,f_y)\} \\ H_z(f_x,f_y) = \mathcal{F}\{h_z(x,y)\} = \exp\left[i2\pi z\sqrt{\lambda^{-2} - f_x^2 - f_y^2}\right] \end{cases} \tag{8}$$

where (f_x, f_y) are the spatial frequencies of the field, H_z is the transfer function of the wave propagation phenomenon, and h_z is the impulse response of the system. Note that since the angular spectrum method is constrained by free-space assumptions, it cannot be employed to compute the optical field propagation through an MLDOE. Therefore, Fourier optics is bounded to propagate a complex field, calculated after the MLDOE, onto a target plane.

4. FDTD RESULTS

In this Section, we use the process described in Fig. 3 to compute the performance of a three-layer F/15 IRG24-IRG27-AgCL MLDOE with 10 diffractive zones. The latter has been optimized using the EST (Eqs. (4) and (5)). The Strehl ratio is accurately retrieved over various wavelengths in the MWIR-LWIR wavebands and displayed in Fig. 5:

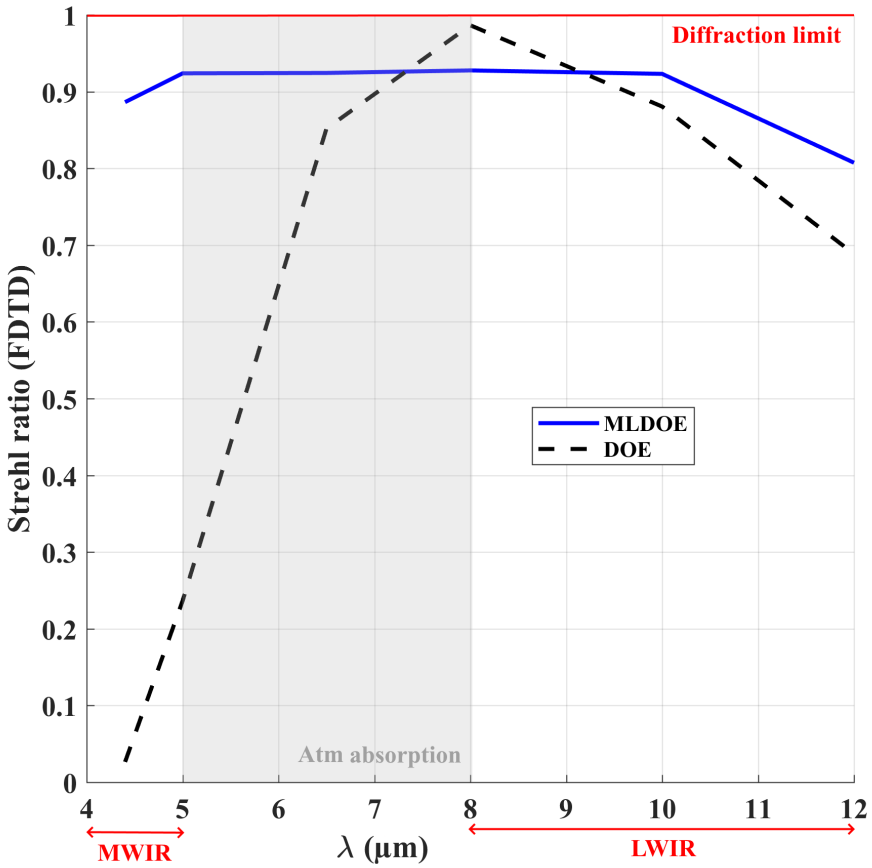

Figure 5: MLDOE Strehl ratio over the MWIR-LWIR bandwidths. The doted black curve displays the performance of a monolayer ZnS DOE. Its efficiency falls-off drastically in MWIR and LWIR, which is not the case for the presented IRG24-IRG27-AgCL MLDOE. The gray area displays the IR atmospheric absorption band.

The optical propagation at $\lambda = 8$ µm is displayed in Fig. 6:

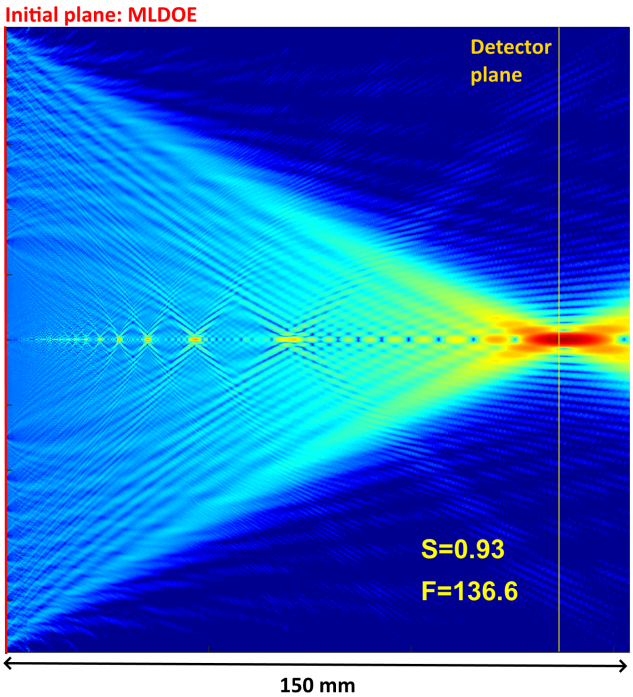

Figure 6: Along axis Fourier optics irradiance propagation. The IRG24-IRG27-AgCl MLDOE lies on the plane $z = 0$ mm and the "best" focal plane is determined using the loop process in Fig. 3. F represents the "best" focal plane while S is the corresponding Strehl ratio value. The presented MLDOE is monofocal.

Finally, the longitudinal chromatic aberration (LCA) is computed over the MWIR-LWIR wavebands, to provide a design-oriented evaluation. In this paper, the LCA is defined as:

$$LCA = f(\lambda) - f(\lambda = 8\mu m) \tag{9}$$

the theoretical LCA is deduced from Eq. 7. The LCA is displayed in Fig. 7 for the studied IRG24-IRG27-AgCl three-layer MLDOE:

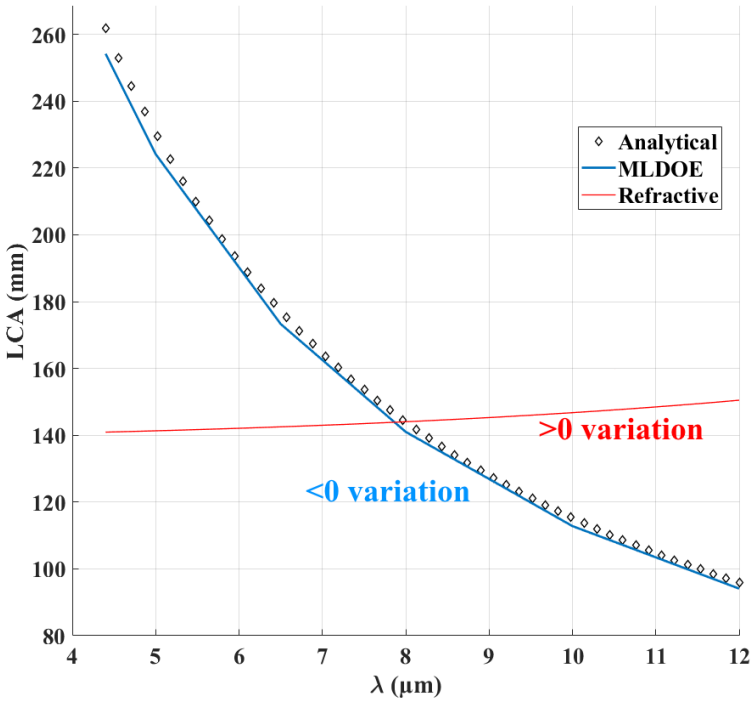

Figure 7: LCA over the MWIR-LWIR wavebands, considering the IRG24-IRG27-AgCl three-layer MLDOE. The theoretical LCA is displayed with black diamonds. Finally, the LCA of a ZnS refractive lens with same F-number is depicted in red for comparison.

From Fig. 7, it can be seen that the MLDOE LCA follows the analytical Eq. (7) and has a negative variation. This is typical for diffractive optics and allows to compensate the refractive LCA (hybrid lens) as depicted in Fig. 8:

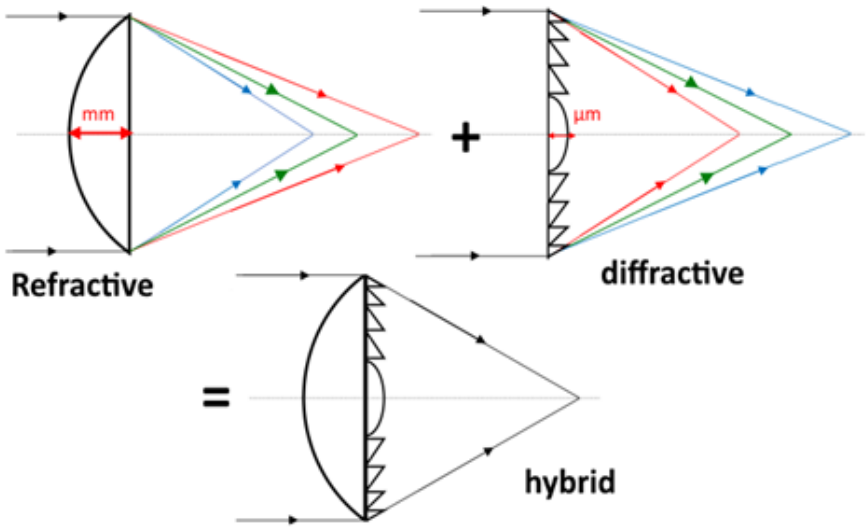

Figure 8: The hybrid combination of refractive and diffractive lenses allow to correct the chromatic aberration with a very compact element.

5. CONCLUSION

The studied multilayer diffractive optical element is a dual-band extension of the classical monolayer diffractive lens (DOE). It is more complex to study but outperforms DOEs in dual-band situations. For Earth observation

purposes, using both MWIR and LWIR wavebands allow to gather high spatial and thermal resolution data. Since these wavebands are tied to the IR source temperature (Planck's law), having two wavebands is promising for wildfire detection, irrigation monitoring, volcano surveillance, etc. The proposed MLDOE has great potential in compact dual-band optical systems since it can be combined with refractive lenses to correct chromatic aberrations, very challenging in such a wide bandwidth. In practice, diffractive grooves are engraved on two refractive lenses (MLDOE layer 1 and 2), resulting in an apochromat hybrid triplet (three wavelength correction) having nearly the size of a doublet. Manufacturing the presented three elements MLDOE is challenging, but the materials have been chosen to be moldable and diamond-turnable, allowing for the generation of complex shapes.

ACKNOWLEDGMENTS

REFERENCES

[1] Sobrino, J. A., Del Frate, F., Drusch, M., Jimenez-Munoz, J. C., Manunta, P., and Regan, A., "Review of Thermal Infrared Applications and Requirements for Future High-Resolution Sensors," *IEEE Transactions on Geoscience and Remote Sensing* **54** (2016).

[2] Sobrino, J. A., Del Frate, F., Drusch, M., Jimenez Munoz, J. C., and Manunta, P., [*Review of High Resolution Thermal Infrared Applications and Requirements: The Fuegosat Synthesis Study*], vol. 17, Springer (2013).

[3] Arieli, Y., Noach, S., Ozeri, S., and Eisenberg, N., "Design of diffractive optical elements for multiple wavelengths," *Applied Optics* **37**(26) (1998).

[4] Swanson, G., "Binary optics technology: Theoretical limits on the diffraction efficiency of multilevel diffractive optical elements," tech. rep., Lincoln Laboratory, Massachusetts Institute of Technology (1991).

[5] Huo, F., Wang, W., and Xue, C., "Limits of scalar diffraction theory for multilayer diffractive optical elements," *Optik* **127** (2016).

[6] Laborde, V., Loicq, J., Hastanin, J., and Habraken, S., "Hybrid ray-tracing/fourier optics method to analyze multilayer diffractive optical elements," *Appl. Opt.* **61**, 4956–4966 (Jun 2022).

[7] Sweeney, C. W. and Sommargren, G. E., "Harmonic diffractive lenses," *Applied Optics* **34**, 2462–2475 (1995).

[8] Faklis, D. and Morris, G. M., "Spectral properties of multiorder diffractive lenses," *Applied Optics* **34**, 2462–2468 (1995).

[9] Laborde, V., Loicq, J., and Habraken, S., "Modeling infrared behavior of multilayer diffractive optical elements using fourier optics," *Appl. Opt.* **60**, 2037–2045 (Mar 2021).

[10] photonic software, O., "Optifdtd." https://optiwave.com/optifdtd-overview/. Accessed: 2022-10-02.

[11] Goodman, J. W., "The angular spectrum of plane waves," in [*Introduction to Fourier Optics*], ch. 3, McGraw-Hill (1996).